

# Feasibility of [<sup>18</sup>F]-2-Fluoro-A85380-PET Imaging of Human Vascular Nicotinic Acetylcholine Receptors In Vivo

Jan Bucorius, MD,\*†‡§|| Christoph Manka, MD,¶# Jörn Schmaljohann, PhD,\*\*  
Venkatesh Mani, PhD,\*††† Daniela Gündisch, PhD,‡‡ James H. F. Rudd, MD, PhD,§§  
Rolf Bippus, PhD,|||| Felix M. Mottaghy, MD,§\*\* Ullrich Wüllner, MD,¶¶  
Zahi A. Fayad, PhD,\*††† Hans-Jürgen Biersack, MD‡  
*New York, New York; Bonn and Aachen Germany; Hilo, Hawaii;  
Cambridge, United Kingdom; and Maastricht, the Netherlands*

**OBJECTIVES** The aim of this feasibility study was to evaluate [<sup>18</sup>F]-2-Fluoro-A85380 for in vivo imaging of arterial nicotinic acetylcholine receptors (nAChRs) in humans. Furthermore, potentially different vascular uptake patterns of this new tracer were evaluated in healthy volunteers and in patients with neurodegenerative disorders.

**BACKGROUND** [<sup>18</sup>F]-2-Fluoro-A85380 was developed for in vivo positron emission tomography (PET) imaging of nAChR subunits in the human brain. These nAChRs are also found in arteries and seem to mediate the deleterious effects of nicotine as a part of tobacco smoke in the vasculature. It has been previously shown that uptake patterns of the radiotracer in the brain differs in patients with neurodegenerative disorders compared with healthy controls.

**METHODS** [<sup>18</sup>F]-2-Fluoro-A85380 uptake was quantified in the ascending and descending aorta, the aortic arch, and the carotids in 5 healthy volunteers and in 6 patients with either Parkinson's disease or multiple system atrophy, respectively, as the maximum target-to-background ratio. The maximal standardized uptake value values, the single hottest segment, and the percent active segments of the [<sup>18</sup>F]-2-Fluoro-A85380 uptake in the arteries were also assessed.

**RESULTS** [<sup>18</sup>F]-2-Fluoro-A85380 uptake was clearly visualized and maximum target-to-background ratio uptake values corrected for the background activity of the tracer showed specific tracer uptake in the arterial walls. Significantly higher uptake values were found in the descending aorta. Comparison between volunteers and patients revealed significant differences, with lower [<sup>18</sup>F]-2-Fluoro-A85380 uptake in the patient group when comparing single arterial territories but not when all arterial territories were pooled together.

**CONCLUSIONS** [<sup>18</sup>F]-2-Fluoro-A85380 can provide specific information on the nAChR distribution in human arteries. Vascular nAChR density seems to be lower in patients with Parkinson's disease or multiple system atrophy. Once confirmed in larger study populations and in the experimental setting, this approach might provide insights into the pathogenic role of nAChRs in the human vasculature. (J Am Coll Cardiol Img 2012;5:528–36) © 2012 by the American College of Cardiology Foundation

From the \*Translational and Molecular Imaging Institute, Mount Sinai School of Medicine, New York, New York; †Department of Radiology, Mount Sinai School of Medicine, New York, New York; ‡Department of Nuclear Medicine, University of Bonn, Bonn, Germany; §Department of Nuclear Medicine, Maastricht University Medical Center, Maastricht, the Netherlands; ||Cardiovascular Research Institute Maastricht (CARIM), Maastricht University Medical Center, Maastricht, the Netherlands; ¶Department of Radiology, Neuroradiology and Interventional Radiology, Gemeinschaftskrankenhaus, Bonn,

Atherosclerosis is one of the leading causes of morbidity and mortality (1). Although cigarette smoke is a complex mixture, nicotine is considered the main toxic and addictive compound of tobacco and a clinical risk factor for atherosclerosis (2–4). Nicotine activates a family of receptors involved in endogenous cholinergic signaling pathways (4). Two different types of nicotinic acetylcholine receptors are distinguished. Whereas the muscle type promotes synaptic transmission at the motor endplate, the neuronal type—originally discovered in the nervous system—is also expressed by several non-neuronal, nonexcitable cells (5). The presence of neuronal nicotinic acetylcholine receptors (nAChRs) at locations unrelated

See page 537

to synaptic activity supports the hypothesis that acetylcholine may have cellular functions mediated by nicotinic receptors (5). nAChRs are present on nerve fibers innervating blood vessels, and there is growing evidence for an nAChR-mediated direct effect of nicotine on the arterial wall (4–6). The presence of nAChRs in a variety of non-neuronal cells, unrelated to synaptic activity, suggests that nicotine causes some of its toxic effects in the respiratory and cardiovascular systems by binding to nAChRs in these organs (5).

Neuronal nAChRs have been shown to assemble as a homogeneous ( $\alpha 7$ -,  $\alpha 9$ -, and  $\alpha 10$ -receptors) or heterogeneous (e.g.,  $\alpha 4\beta 2$ -receptor) pentamer of  $\alpha$ - and  $\beta$ -subunits, including  $\alpha 2$ – $\alpha 7$  and  $\beta 2$ – $\beta 4$ .  $\alpha 7$ -,  $\alpha 9$ -, and  $\alpha 10$ -subunits are also able to assemble in functional  $\alpha$ -heteropentamers (4,7–9). The composition of subunits determines ligand specificity, ligand affinity, cation permeability, and channel kinetics (10).

$\alpha 4\beta 2$  nAChRs can be noninvasively visualized with  $2$ - $^{18}\text{F}$ -Fluoro-3-[2(S)-2-azetidylmethoxy]pyridine

( $^{18}\text{F}$ ]-2-Fluoro-A85380), a radiolabeled receptor ligand with high affinity to  $\beta 2$  subunits (11).  $^{18}\text{F}$ ]-2-Fluoro-A85380 is the first radiotracer allowing subtype-selective investigation of nAChRs in vivo in humans by using positron emission tomography (PET) imaging, primarily in the brain (11,12). It was shown that there is a broad reduction of the  $\alpha 4\beta 2$  nAChR availability in patients with Parkinson's disease (PD) without clinically manifested dementia or depression compared with healthy volunteers (13). In contrast, in smokers without any neurological or medical disease, nAChRs in the brain were up-regulated compared with nonsmokers (14).

Because of the well-known similarity between nAChRs both within and outside the brain,  $^{18}\text{F}$ ]-2-Fluoro-A85380 might also allow in vivo assessment of nAChRs outside the brain. This is further supported by the fact that it seemed feasible to image human cardiac nAChRs (5,15,16).

The aim of the current study was to evaluate the feasibility of  $^{18}\text{F}$ ]-2-Fluoro-A85380 to image the nicotinic  $\alpha 4\beta 2$  receptor subunits in the human vasculature. Furthermore, we assumed that the vascular uptake patterns of the radiotracer might be different in patients with neurodegenerative disorders. Once confirmed to be feasible for imaging nAChRs in the vessels,  $^{18}\text{F}$ ]-2-Fluoro-A85380-PET imaging might therefore not only allow for in vivo assessment of the receptor distribution in the vasculature of subjects with and without neurodegenerative disorders but also to evaluate receptor density in the vessels, as previously seen in the human brain of smokers (14). The latter could therefore also provide insights regarding nAChR-mediated deleterious effects of nicotine.

#### ABBREVIATIONS AND ACRONYMS

CT = computed tomography

JV = jugular vein

MSA = multiple system atrophy

nAChR = nicotinic acetylcholine receptor

PAS = percent active segments

PD = Parkinson's disease

PET = positron emission tomography

ROI = region of interest

SHS = single hottest segment

SUV = standardized uptake value

SVC = superior vena cava

TBR = target-to-background ratio

Germany; #Department of Radiology, University of Bonn, Bonn, Germany; \*\*Department of Nuclear Medicine, RWTH Aachen, Aachen, Germany; ††Department of Cardiology, Zena and Michael A. Wiener Cardiovascular Institute and Marie-Josée and Henry R. Kravis Cardiovascular Health Center, Mount Sinai School of Medicine, New York, New York; ‡‡College of Pharmacy, University of Hawaii at Hilo, Hilo, Hawaii; §§Division of Cardiovascular Medicine, University of Cambridge, Cambridge; United Kingdom; |||Department of Molecular Imaging Systems, Philips Research Europe, Aachen, Germany; and ¶¶Department of Neurology, University of Bonn, Bonn, Germany. Work in this paper was partly supported by the NIH Cambridge Biomedical Research Centre (Dr. Rudd). Partial support was also provided by NIH/NHLBI R01 HL071021 (Dr. Fayad). This study was supported by DFG (Deutsche Forschungsgemeinschaft) SP 1226 "Nicotine" (Wu184/8-1). Dr. Willner has served as a consultant and lecturer and on advisory boards for Boehringer-Ingelheim, GlaxoSmithKline, Lifescience KG, Lundbeck AG, Teva Pharma, and UCB Pharma and has received research funding from Bundesministerium für Bildung und Forschung, Deutsche Forschungsgemeinschaft, National Ataxia Foundation, deutsche Parkinson Vereinigung, and the European Union. All other authors have reported that they have no relationships relevant to the contents of this paper to disclose. H. William Strauss, MD, served as Guest Editor for this paper.

Manuscript received May 31, 2011; revised manuscript received October 20, 2011, accepted November 28, 2011.

## METHODS

**Study design.** This feasibility study evaluating the nAChR density in human brain and vasculature of patients with neurodegenerative disorders and healthy controls was conducted at the Department of Nuclear Medicine, University of Bonn (Bonn, Germany). The local institutional review board as well as the federal authorities approved the study. All individuals provided written informed consent. The brain part of the results has been published separately (17).

Five healthy volunteers and 6 patients with PD or multiple system atrophy (MSA) were evaluated (mean age  $62.6 \pm 9.1$  years); none had cardiac disease. None of the study subjects ever smoked or received cardiovascular medications.

PD or MSA was diagnosed by an experienced movement disorder specialist (Dr. Wüllner) according to the UK Disease Society Brain Bank criteria or the MSA consensus criteria (18,19). All PD and MSA patients received combinations of levodopa and various dopamine agonists. Four patients additionally received antidepressants, and 2 received amantadine. PET imaging was performed in a defined “off” with the last medication >12 h before radiopharmaceutical application.

**Radiochemistry.** [ $^{18}\text{F}$ ]-2-Fluoro-A85380 was prepared as a sterile, apyrogenic solution in phosphate buffer (pH 7.0) as described previously (11). The aqueous [ $^{18}\text{F}$ ]fluoride solution was dried in 3 ml of acetonitrile, 25 mg (66  $\mu\text{mol}$ ) of Kryptofix<sup>TM</sup> K222, and 2.8 mg (20  $\mu\text{mol}$ ) of  $\text{K}_2\text{CO}_3$ . Two milligrams (4.3  $\mu\text{mol}$ ) of 2-trimethylammonium-3-(1-tert-

butoxycarbonyl-2(S)-azetidiny-methoxy)-pyridine trifluoromethanesulfonate dissolved in 1 ml of dimethyl sulfoxide were added and heated at  $135^\circ\text{C}$  for 5 min. After dilution with 4 ml of water, the reaction mixture was passed through an ICH cartridge (Alltech ICH, Grace Davison Discovery Science, Deerfield, Illinois), SepPak QMA cartridge (Waters Corporation, Milford, Massachusetts), and Sep Pak RP18 cartridge (Waters Corporation). The cartridges were washed with 2 ml of water, and the intermediate product [ $^{18}\text{F}$ ]-N-BOC-2F-A85380 was eluted from the C18-cartridge with 1 ml of ethanol. Cleavage of the BOC group was performed by adding 1 ml 0.2 M of hydrochloric acid and simultaneous evaporation of ethanol. After adding 4 ml of phosphate buffer, the product [ $^{18}\text{F}$ ]-2F-A85380 was filtrated over a sterile filter (0.2  $\mu\text{m}$ ) and collected in a sterile vial. An aliquot was analyzed by using high-performance liquid chromatography and thin-layer chromatography. The specific activity of [ $^{18}\text{F}$ ]-2-Fluoro-A85380 was determined at the end-of-synthesis to range from 330 to 820  $\text{GBq}/\mu\text{mol}$  (8.9 to 22.2  $\text{Ci}/\mu\text{mol}$ ) with a radiochemical purity >95% (11,14).

It has previously been shown that [ $^{18}\text{F}$ ]-2F-A85380 has a rapid clearance from the blood with a low rate (<15%) of metabolites at 120 min (14). The tracer is primarily eliminated renally (12). Figure 1 shows the [ $^{18}\text{F}$ ]-2F-A85380 whole body distribution.

**[ $^{18}\text{F}$ ]-2-Fluoro-A85380-PET/computed tomography imaging.** All subjects underwent PET/computed tomography (CT) scanning (biograph, Siemens

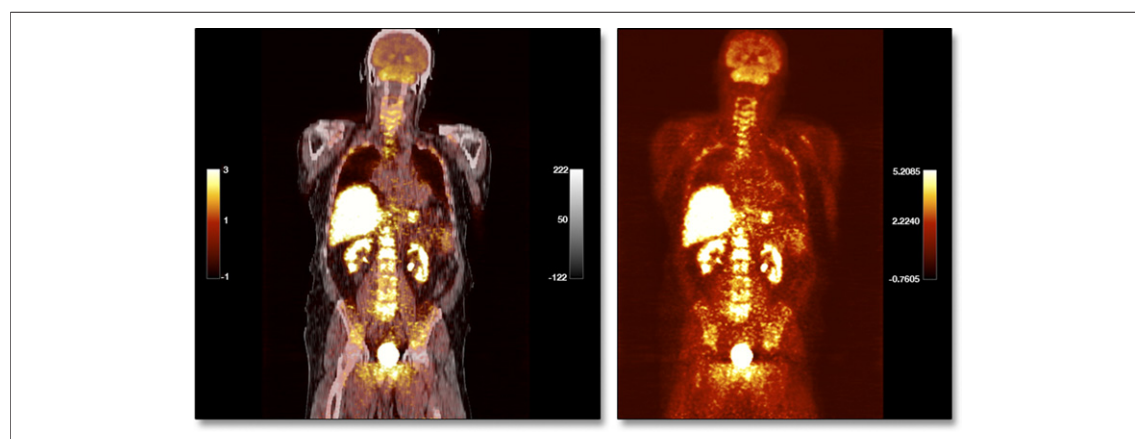


**Figure 1.** Whole Body [ $^{18}\text{F}$ ]-2-Fluoro-A85380 PET Image

The whole body [ $^{18}\text{F}$ ]-2-Fluoro-A85380 distribution is shown on coronal fused positron emission tomography (PET)/computed tomography (CT) as well as on PET-only images. Intense tracer uptake in the liver, the kidneys, and the bladder as well as in the vertebrae is observed.

Medical Systems, Erlangen, Germany). After administration of an intravenous bolus injection of  $371.2 \pm 58.1$  MBq of [ $^{18}\text{F}$ ]-2-Fluoro-A85380, all patients rested comfortably for 49 to 92 min ( $74.9 \pm 11.6$  min) before acquisition. A whole body PET/CT scan with 5 to 6 bed positions, each with 3-min acquisition time, was performed. PET was acquired in 3-dimensional mode using a matrix of  $256 \times 256$ , followed by reconstruction of the data using iterative reconstruction. The reconstructed resolution of the PET system was 6.7 mm. A low-dose, noncontrast-enhanced CT imaging protocol (130 kV, 40 mAs; 2 helical slices, 5-mm slice thickness) was used, ensuring a diagnostic quality of the images and providing a reasonable contrast to delineate and judge the targeted structures such as the arterial vessel walls and the lumen of the superior vena cava (SVC) and both jugular veins (JVs) to assure an appropriate estimation of the blood pool activity of the tracer. CT images were reconstructed onto a  $512 \times 512$  matrix, and these data, expressed as Hounsfield units, were converted into 511 keV equivalent attenuation factors for attenuation corrections.

**Image analysis.** All scans were analyzed in consensus by 2 experienced readers (J.B., C.M.). Image analysis was performed on an Imalytics Research Workspace (Imalytics 2.1, Philips Technologies GmbH Innovative Technologies, Aachen, Germany). Vascular tracer uptake was measured according to established methods that have been published previously (20).

Following a standardized image analysis protocol, both carotids, the ascending and descending aorta, the aortic arch, and both the JV and SVC were evaluated. For the carotid arteries, only the common carotid artery up to the bifurcation was analyzed on both sides of the neck. Slices where the anatomy of the distinct vessel could not be identified with certainty were excluded. Arterial [ $^{18}\text{F}$ ]-2-Fluoro-A85380 uptake was quantified by drawing a region of interest (ROI) around each artery on every slice of the co-registered transaxial PET/CT images (Fig. 2) (20,21). Next, the maximal arterial standardized uptake value ( $\text{SUV}_{\text{max}}$ ) was calculated within the region of interest of every slice of the vessel. By averaging the maximum SUV values of all arterial slices of each of the analyzed vessels, a  $_{\text{mean}}\text{SUV}_{\text{max}}$  value was derived for an individual vessel. The maximal arterial target-to-background ratio ( $\text{TBR}_{\text{max}}$ ) was then calculated by correcting the  $\text{SUV}_{\text{max}}$  for blood activity. This was done by dividing the  $\text{SUV}_{\text{max}}$  values in a distinct artery by

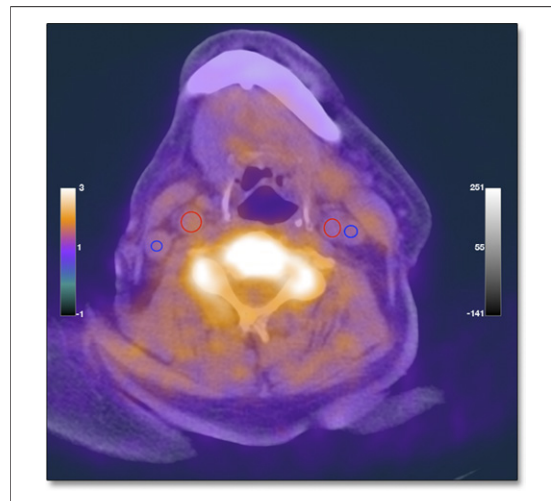


**Figure 2. [ $^{18}\text{F}$ ]-2-Fluoro-A85380 PET Image Analysis**

This figure shows one slice of the fused PET/CT images of the neck in transaxial view. Regions of interest (ROIs) drawn around the outer border of the vessel walls of the left and right common carotid artery (red ROIs) as well as for evaluation of the [ $^{18}\text{F}$ ]-2-Fluoro-A85380 blood pool activity, within the lumen of both jugular veins (blue ROIs; maximal standardized uptake value [ $\text{SUV}_{\text{max}}$ ],  $\text{SUV}_{\text{mean}}$ , and diameter of all ROIs were evaluated). A higher arterial [ $^{18}\text{F}$ ]-2-Fluoro-A85380 uptake is easily visualizable in the right carotid artery compared with the left carotid artery ( $\text{SUV}_{\text{max}}$  1.79 vs. 1.23) whereas similar  $\text{SUV}_{\text{mean}}$  values are seen for the [ $^{18}\text{F}$ ]-2-Fluoro-A85380 blood pool activity in both jugular veins (JV) ( $\text{SUV}_{\text{mean}}$  right JV: 1.26;  $\text{SUV}_{\text{mean}}$  left JV 1.22). Abbreviations in Figure 1.

the average blood  $\text{SUV}_{\text{mean}}$ , estimated from both JVs (for correcting the carotid arteries) or the SVC (for correcting the ascending and descending aorta as well as the aortic arch), respectively. Based on previously published data on  $^{18}\text{F}$ -FDG-PET, this correction is considered to be a reflection of arterial [ $^{18}\text{F}$ ]-2-Fluoro-A85380 uptake (20,21). For evaluation of the mean [ $^{18}\text{F}$ ]-2-Fluoro-A85380 blood pool uptake (mean  $\text{SUV}_{\text{mean}}$ ), at least six 3- to 4-mm ROIs were placed in consecutive slices of both, the JVs or the SVC, and averaged. Corrected  $\text{SUV}_{\text{max}}$  values were averaged to derive a  $_{\text{mean}}\text{TBR}_{\text{max}}$  for all of the analyzed arteries. In addition, we identified the single hottest segment (SHS), defined as the highest  $\text{TBR}_{\text{max}}$  value of the arteries as well as the percent active segments (PAS) of each arterial vessel. PAS reflects the percentage of all segments of a distinct artery above a predefined threshold, namely  $\text{TBR}_{\text{max}} > 1.32$  (ascending aorta),  $> 1.71$  (descending aorta),  $> 1.68$  (aortic arch), and  $> 1.27$  (carotids), respectively. These thresholds were determined by calculating the median of all  $_{\text{mean}}\text{TBR}_{\text{max}}$  values of the 4 different arterial territories across all subjects.

**Statistical analysis.** A one-way analysis of variance with the appropriate adjustment for multiple comparisons was used to test for differences of the [ $^{18}\text{F}$ ]-2-Fluoro-A85380 uptake values between all vessels in the total study population. Post hoc analyses were performed using the Tukey test. The Student *t* test was performed after confirming normal distribution to compare [ $^{18}\text{F}$ ]-2-Fluoro-A85380 uptake values for the arterial territories altogether as well as for each of the arterial territories between the group of volunteers and the group of patients with neurological disorders. After confirming normal distribution, Pearson correlation coefficients (*r*) were calculated to evaluate a potential association between the age and the body mass index of the subjects and the different uptake parameters.

All statistical analyses were performed using SPSS version 16.0 (SPSS Inc., Chicago, Illinois).

## RESULTS

No pharmacological effects (e.g., changes in heart or respiration rate or blood pressure) were observed after administration of [ $^{18}\text{F}$ ]-2-Fluoro-A85380. In the current study, the administered mass doses were 0.5 to 1.5 nmol and thus <1% of the dose, which led to pharmacological effects in nonhuman primates (22).

In 2 of 11 subjects, the anatomy of the left carotid artery could not be clearly identified on the CT scan and was therefore excluded from further analyses. However, in each case, the anatomy of the right carotid artery was assessable and rendered data for

statistical analyses of the carotids in both subjects. Patient characteristics are shown in Table 1.

In all subjects, [ $^{18}\text{F}$ ]-2-Fluoro-A85380 uptake in the arteries as well as in the JV and SVC could be easily identified by visual inspection. Furthermore, with the exception of the 2 left carotid arteries as mentioned earlier, ROIs for semi-quantitative analyses of the [ $^{18}\text{F}$ ]-2-Fluoro-A85380 uptake could be precisely placed in all analyzed vessels.

No correlation was observed between the 4 [ $^{18}\text{F}$ ]-2-Fluoro-A85380 uptake parameters and the age of the subjects. Body mass index significantly correlated with the  $\text{mean SUV}_{\text{max}}$  in the ascending aorta ( $r = 0.81$ ;  $p = 0.004$ ), in the aortic arch ( $r = 0.86$ ;  $p = 0.001$ ), and in the carotids ( $r = 0.64$ ;  $p = 0.048$ ), as well as with the  $\text{mean SUV}_{\text{mean}}$  in the JV ( $r = 0.64$ ;  $p = 0.046$ ) and the SVC ( $r = 0.74$ ;  $p = 0.014$ ).

Differences between the [ $^{18}\text{F}$ ]-2-Fluoro-A85380 uptake of each arterial territory in the total study population are depicted in Figures 3 and 4. Uptake values for the arterial territories altogether as well as for each of the 4 arterial territories in the subgroups of volunteers and patients with PD or MSA, respectively, are provided in Table 2. Considering the total study population, all [ $^{18}\text{F}$ ]-2-Fluoro-A85380 uptake parameters except the PAS values were shown to be highest in the descending aorta, followed by the aortic arch, the ascending aorta, and the carotids. Statistically significant differences were observed with regard to the  $\text{mean SUV}_{\text{max}}$ , the  $\text{mean TBR}_{\text{max}}$ , and the SHS values between the descending aorta and the ascending aorta as well as the carotids (Fig. 3). In contrast, highest PAS values were

**Table 1. Patient Characteristics**

Subject	Disorder	Sex	Age (yrs)	Height (m)	Weight (kg)	BMI (kg/m <sup>2</sup> )
1	Volunteer	M	47	1.91	79	21.7
2	Volunteer	M	61	1.88	90	25.5
3	Volunteer	F	66	1.72	62	21.0
4	Volunteer	M	60	1.65	78	28.7
5	Volunteer	F	80	NA	80	NA
Mean $\pm$ SD	—	—	62.7 $\pm$ 11.6	1.79 $\pm$ 0.13	77.8 $\pm$ 10.1	24.2 $\pm$ 3.6
6	PD	M	70	1.73	95	31.7
7	PD	F	66	1.73	55	18.4
8	PD	M	70	1.74	82	27.1
9	MSA	M	60	1.73	80	26.7
10	MSA	F	60	1.60	54	21.1
11	MSA	F	50	1.68	60	21.3
Mean $\pm$ SD	—	—	62.6 $\pm$ 7.5	1.70 $\pm$ 0.05	71.0 $\pm$ 17.0	24.4 $\pm$ 5.0
Total mean $\pm$ SD	—	—	62.6 $\pm$ 9.1	1.74 $\pm$ 0.09	74.1 $\pm$ 14.1	24.3 $\pm$ 4.2

BMI = body mass index; MSA = multiple system atrophy; NA = not available; PD = Parkinson's disease.

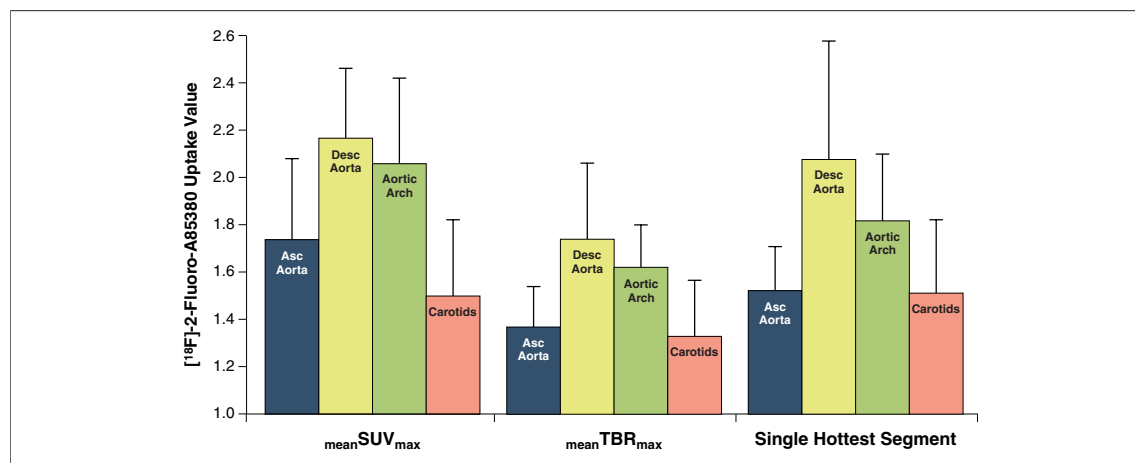


**Figure 3. Average mean SUV<sub>max</sub>, mean TBR<sub>max</sub>, and Single Hottest Segment Values in Each Arterial Territory Analyzed**

Comparison of [<sup>18</sup>F]-2-Fluoro-A85380 uptake values revealed the following statistically significant differences (p values are given for significant differences only) between the different arterial territories: mean SUV<sub>max</sub>—descending aorta (DescAorta) versus ascending aorta (AscAorta) p = 0.019; DescAorta versus Carotids p < 0.0001; AorticArch versus Carotids p = 0.001; mean TBR<sub>max</sub>—DescAorta versus AscAorta p = 0.003; DescAorta versus Carotids p = 0.001; Single Hottest Segment—DescAorta versus AscAorta p = 0.002; DescAorta versus Carotids p = 0.002. TBR = target-to-background ratio; other abbreviations as in Figure 2.

found for the carotids followed by the ascending and descending aorta and the aortic arch. However, these differences were not statistically significant (Fig. 4).

## DISCUSSION

Over the past decade, interest has increased in noninvasive functional imaging of vascular inflammation or different parts of the underlying complex

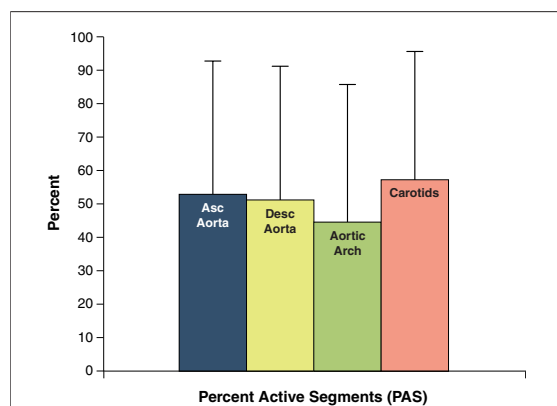


**Figure 4. Average PAS Values in Each Arterial Territory Analyzed**

Percent active segments (PAS) are defined as the percentage of segments with TBR<sub>max</sub> >1.32 (AscAorta), >1.71 (DescAorta), >1.68 (AorticArch), and >1.27 (Carotids), respectively. No statistically significant differences between the arterial territories were seen with regard to PAS. Abbreviations as in Figure 3.

pathological processes of atherosclerosis by means of PET (23).

Imaging of nAChRs in the vasculature might be a promising approach because the availability of evidence, which suggests that this type of receptor can be found in vascular cells such as smooth muscle, endothelial, or immune cells, including lymphocytes, monocytes, and platelets (6,24–26). In the vascular system, α3, α4, α5, α7, and α10 nicotinic subunits were previously found in smooth muscle cells (5,27). Although the α4-subunit is not detected in muscle, kidney, or lung arteries, every αnAChR subunit has been detected in the thoracic aorta except the α9-subunit (4,27). Interestingly, the α4-subunit was also detected in the abdominal, but not ascending, aorta and the pulmonary trunk (4). The α7-nAChR is expressed on a majority of smooth muscle cells and intrapulmonary arteries with the exception of the renal circulation (6,27). Several lines of evidence show that α3-, α5-, α7-, α10-, and β2–β4-subunits are also found on human vascular endothelial cells (5,24,28). Furthermore, immunohistochemical staining for nAChRs isoforms using nAChR subunit-specific antibodies revealed α3, α4, α7, β2 and β4 to be expressed by human umbilical vein endothelial cells (29). It was also found that coronary microvascular endothelial cells of the rat expressed messenger ribonucleic acid for the subunits α2, α3, α4, α5, and α7 as well as β2 and β4 of the nAChRs, whereas the β3-subunit was not detected (30). Interestingly, it has been

**Table 2. [<sup>18</sup>F]-2-Fluoro-A85380 Uptake Values of All and Each of the Different Arterial Territories Between Volunteers and Patients With PD or MSA, Respectively**

[ <sup>18</sup> F]-2-Fluoro-A85380 Uptake Value	Volunteers	Patients (PD + MSA)	p Value
<b>All arterial territories</b>			
mean SUV <sub>max</sub>	1.84 ± 0.39	1.89 ± 0.45	NS
mean TBR <sub>max</sub>	1.59 ± 0.24	1.45 ± 0.31	NS
PAS	63.5 ± 31.6	41.6 ± 41.2	NS
SHS	1.84 ± 0.32	1.65 ± 0.46	NS
<b>Ascending aorta</b>			
mean SUV <sub>max</sub>	1.79 ± 0.29	1.71 ± 0.4	NS
mean TBR <sub>max</sub>	1.51 ± 0.14	1.26 ± 0.07	0.003
PAS	81.7 ± 29.1	28.9 ± 30.7	0.017
SHS	1.65 ± 0.19	1.41 ± 0.11	0.025
<b>Descending aorta</b>			
mean SUV <sub>max</sub>	2.04 ± 0.25	2.29 ± 0.29	NS
mean TBR <sub>max</sub>	1.72 ± 0.11	1.76 ± 0.44	NS
PAS	54.1 ± 29.0	48.9 ± 49.5	NS
SHS	2.03 ± 0.12	2.13 ± 0.69	NS
<b>Aortic arch</b>			
mean SUV <sub>max</sub>	2.07 ± 0.35	2.04 ± 0.39	NS
mean TBR <sub>max</sub>	1.74 ± 0.11	1.52 ± 0.15	0.026
PAS	69.1 ± 31.3	24.4 ± 38.1	NS
SHS	2.05 ± 0.16	1.63 ± 0.21	0.005
<b>Carotids</b>			
mean SUV <sub>max</sub>	1.45 ± 0.36	1.53 ± 0.31	NS
mean TBR <sub>max</sub>	1.39 ± 0.34	1.28 ± 0.13	NS
PAS	49.2 ± 35.4	64.4 ± 41.6	NS
SHS	1.62 ± 0.44	1.42 ± 0.14	NS

Values are mean ± SD. Each of the 4 groups in all arterial territories comprises 1 of the different [<sup>18</sup>F]-2-Fluoro-A85380 uptake values of all of the 4 different arterial territories from each patient. Therefore, for each patient, 4 different values for each uptake parameter from the 4 different territories entered further analyses. No statistical significant differences were found between both groups of subjects for all of the 4 different [<sup>18</sup>F]-2-Fluoro-A85380 uptake values when pooling all of the 4 arterial territories. Comparing each of the arterial territories between both groups revealed significantly lower uptake parameters in the group of patients with neurological disorders in the ascending aorta (mean TBR<sub>max</sub>, PAS, SHS) and in the aortic arch (mean TBR<sub>max</sub>, SHS). MSA = multiple system atrophy; PAS = percent active segments; PD = Parkinson's disease; SHS = single hottest segment; SUV<sub>max</sub> = maximal standardized uptake value; TBR = target-to-background ratio.

shown previously that the deleterious effects of nicotine, as part of tobacco smoke, on the arterial wall might be mediated by exactly those nAChRs (4–6,24–26,28–30). These mediating effects of nAChRs are related to the control of smooth muscle cell proliferation and angiogenesis, of endothelial cell proliferation by, among others, inducing the expression of endothelial growth factors and up-regulating endothelial nitric oxide synthase in endothelial cells, invasion, and angiogenesis, as well as by activation of immune cells such as lymphocytes (3,6,24–27,29,31,32).

It was previously shown that smoking up-regulates  $\alpha 4\beta 2$  nAChRs in the human brain (14). Translating these findings to the vasculature by

using noninvasively functional imaging of the nAChRs can provide insights into the pathogenic role of nicotine in the atherosclerotic process by confirming a higher number of nAChRs in the vessels of smokers. Proving the presence and the density of nAChRs in the vasculature by using noninvasive functional imaging would provide the rationale for therapeutic modulation of the aforementioned nAChRs-mediated processes, as already shown in an experimental setting (32). Whereas nAChR antagonists such as mecamylamine were previously shown to have anti-angiogenic properties in an animal model of choroidal neovascularization, nAChR agonist such as choline, in contrast, enhanced angiogenesis and restored blood flow in rat models of myocardial infarction. They may therefore facilitate revascularization in ischemic tissues (33,34).

The data of the current study seem to indicate that visualization of  $\alpha 4\beta 2$  nAChRs in arterial vessels using [<sup>18</sup>F]-2-Fluoro-A85380 might be feasible. This result is even more striking because it has been previously shown that among nAChRs, those containing  $\alpha 4$  and  $\beta 2$  subunits, and probably those subtypes containing  $\beta 2$  in combination with other subunits, have the highest affinity for nicotine. They might therefore be among the most important mediators of the nicotine-related pathogenic impact on atherosclerosis (16). By correcting the [<sup>18</sup>F]-2-Fluoro-A85380 SUVs for the underlying unspecific background activity, we found the calculated TBRs still to be higher than the underlying blood pool [<sup>18</sup>F]-2-Fluoro-A85380 activity. This clearly indicates a specific [<sup>18</sup>F]-2-Fluoro-A85380 uptake in the arterial vessel wall, as, in case of unspecific tracer accumulation, one has to assume a TBR equal to  $\leq 1$ . We found the [<sup>18</sup>F]-2-Fluoro-A85380 uptake parameters to be highest in the descending aorta. This is impressive because previous data from an animal study by Brüggmann et al. (4) revealed the highest distribution of the  $\alpha 4$  subunit in vascular smooth muscle cells distal to the ascending aorta. Because [<sup>18</sup>F]-2-Fluoro-A85380 visualizes  $\alpha 4$  and  $\beta 2$  subunits, our data seem to confirm these findings in humans.

[<sup>18</sup>F]-2-Fluoro-A85380 was recently developed to noninvasively visualize  $\alpha 4\beta 2$  nAChRs in the central nervous system. Because of its high affinity and selectivity to these distinct nAChR subtypes, it could be proven to be highly suitable for in vivo assessment of the  $\alpha 4\beta 2$  nAChR availability in the human brain (12). It was recently shown that in patients with Alzheimer's disease or PD and mild

cognitive impairment, the availability of the  $\alpha4\beta2$  nAChRs was decreased (13,35). A reduced availability of nAChRs in the brain could also be shown in our patient population when evaluating the tracer uptake patterns and therefore the nAChR distribution in the brain. These data were previously published by our group (17). We found a significant reduction of radioactivity intra-individually in the left compared with the right temporal cortex. Similarly, we also observed a minor decrease of radioactivity in the putamen of patients with PD and MSA. MSA patients, although of the parkinsonian type, showed a significant reduction of [ $^{18}\text{F}$ ]-2-Fluoro-A85380 accumulation in the cerebellum (17). Our data seem to be in accordance with the finding of diminished  $\alpha4\beta2$  nAChR availability in the brain in patients with neurodegenerative disorders; statistically significant differences of the [ $^{18}\text{F}$ ]-2-Fluoro-A85380 uptake between volunteers and patients with neurological disorders (lower uptake) were observed. Because this significant reduction of the [ $^{18}\text{F}$ ]-2-Fluoro-A85380 uptake was only seen in 2 of the 4 different arterial territories of the patients and was not seen at all when pooling the territories, our data seem to indicate that different parts of the vascular system might be differently affected by neurodegenerative changes, if at all. The finding of an altered vascular nAChR density in patients with neurodegenerative disorders is intriguing because the results of the current study might also indicate a usefulness of [ $^{18}\text{F}$ ]-2-Fluoro-A85380 vascular imaging to provide insights into the pathogenesis of PD or Alzheimer's disease. This cannot be overemphasized because the vascular role in the pathologic process of Alzheimer's disease became more and more evident over the past years, and there has been continuous debate over the last 75 years about the existence of vascular parkinsonism as opposed to idiopathic PD (36–38). Because the differentiation of vascular parkinsonism from idiopathic PD remains a challenge, [ $^{18}\text{F}$ ]-2-Fluoro-A85380 vascular PET imaging might be-

come a possible diagnostic measure for this purpose in the future (38).

**Study limitations.** The study population, both of patients with PD and MSA, respectively, as well as healthy volunteers was rather small, and heterogeneous limiting to some degree its conclusions. However, it was designed as a feasibility study of arterial nAChR imaging with the recently developed [ $^{18}\text{F}$ ]-2-Fluoro-A85380 PET tracer. Future studies will be needed to confirm the correlation between the vascular [ $^{18}\text{F}$ ]-2-Fluoro-A85380 uptake and the presence of  $\alpha4\beta2$  nAChRs by using histology. As a further limitation, no dynamic vascular PET imaging of [ $^{18}\text{F}$ ]-2-Fluoro-A85380 was performed. However, in this feasibility study, we found an easily and clearly visualizable TBR of the tracer >70 min after injection. Furthermore, semi-quantitative analyses of the [ $^{18}\text{F}$ ]-2-Fluoro-A85380 uptake with appropriate correction for the nonspecific background activity of the tracer also indicated specific tracer uptake in the arterial vessels. Finally, subjects did not have established vascular disease. Therefore, at this time, we cannot correlate the tracer uptake in the vessels with clinical cardiovascular risk factors except for body mass index. This issue will be addressed by future trials with a dedicated and well-powered study population.

## CONCLUSIONS

The results of the feasibility study seem to indicate a specific uptake of [ $^{18}\text{F}$ ]-2-Fluoro-A85380 for in vivo visualization of  $\alpha4\beta2$  nAChRs in human arterial vessels. Furthermore, vascular [ $^{18}\text{F}$ ]-2-Fluoro-A85380 imaging might also provide information on the vascular role in neurodegenerative disorders such as PD or Alzheimer's disease.

**Reprint requests and correspondence:** Dr. Jan Bucerius, Translational and Molecular Imaging Institute, Mount Sinai School of Medicine, One Gustave L. Levy Place, P.O. Box 1234, New York, New York 10029. *E-mail:* jan.bucerius@mumc.nl.

## REFERENCES

1. Lloyd-Jones D, Adams R, Carnethon M, et al. American Heart Association Statistics Committee and Stroke Statistics Subcommittee. Heart disease and stroke statistics—2009 update: a report from the American Heart Association Statistics Committee and Stroke Statistics Subcommittee. *Circulation* 2009;119:480–6.
2. Bolego C, Poli A, Paoletti R. Smoking and gender. *Cardiovasc Res* 2002; 53:568–76.
3. Conklin BS, Zhao W, Zhong DS, Chen C. Nicotine and cotinine up-regulate vascular endothelial growth factor expression in endothelial cells. *Am J Pathol* 2002;160:413–8.
4. Brüggmann D, Lips KS, Pfeil U, Haberberger RV, Kummer W. Multiple nicotinic acetylcholine receptor  $\alpha$ -subunits are expressed in the arterial system of the rat. *Histochem Cell Biol* 2002;118: 441–7.

5. Conti-Fine BM, Navaneetham D, Lei S, Maus AD. Neuronal nicotinic receptors in non-neuronal cells: new mediators of tobacco toxicity? *Eur J Pharmacol* 2000;393:279-94.
6. Egleton RD, Brown KC, Dasgupta P. Angiogenic activity of nicotinic acetylcholine receptors: implications in tobacco-related vascular diseases. *Pharmacol Ther* 2009;121:205-23.
7. Listerud M, Brussaard AB, Devay P, Coleman DR, Role LW. Functional contribution of neuronal AchR subunits revealed by anti-sense oligonucleotides [published correction in *Science* 1992;255:12]. *Science* 1991;254:1518-21.
8. Vernallis AB, Conroy WG, Berg DK. Neurons assemble acetylcholine receptors with as many as three kinds of subunits while maintaining subunit segregation among receptor subtypes. *Neuron* 1993;10:451-64.
9. Sgard F, Charpantier E, Bertrand S, et al. A novel human nicotinic receptor subunit, alpha10, that confers functionality to the alpha9-subunit. *Mol Pharmacol* 2002;61:150-9.
10. Buisson B, Picard F, Bertrand D. Neuronal nicotinic acetylcholine receptors: from biophysical properties to human diseases. In: Clementi F, Gotti C, Fornasari D, editors. *Neuronal Nicotinic Receptors*. Springer, Berlin Heidelberg New York, 2000:272-99.
11. Schmaljohann J, Minnerop M, Karwath P, et al. Imaging of central nAChReceptors with 2-[<sup>18</sup>F]F-A85380: optimized synthesis and in vitro evaluation in Alzheimer's disease. *Appl Rad Iso* 2004;61:1235-40.
12. Kimes AS, Horti AG, London ED, et al. 2-[<sup>18</sup>F]F-A-85380: PET imaging of brain nicotinic acetylcholine receptors and whole body distribution in humans. *FASEB J* 2003;17:1331-3.
13. Meyer PM, Streckler K, Kendziorra K, et al. Reduced alpha4beta2\*-nicotinic acetylcholine receptor binding and its relationship to mild cognitive and depressive symptoms in Parkinson disease. *Arch Gen Psychiatry* 2009;66:866-77.
14. Wüllner U, Gündisch D, Herzog H, et al. Smoking upregulates alpha4beta2\* nicotinic acetylcholine receptors in the human brain. *Neurosci Lett* 2008;430:34-7.
15. Bucerius J, Joe AY, Schmaljohann J, et al. Feasibility of 2-deoxy-2-[<sup>18</sup>F]fluoro-D-glucose-A85380-PET for imaging of human cardiac nicotinic acetylcholine receptors in vivo [published correction in *Clin Res Cardiol* 2006;95:354]. *Clin Res Cardiol* 2006;95:105-9.
16. Mukhin AG, Gündisch D, Horti AG, et al. 5-Iodo-A-85380, an alpha4beta2 subtype-selective ligand for nicotinic acetylcholine receptors. *Mol Pharmacol* 2000;57:642-9.
17. Wüllner U, Bucerius J, Gündisch D, et al. PET-Imaging of alpha4beta2\* nicotinic acetylcholine receptors in the central and peripheral nervous system. *Akt Neurol* 2006;33:P638.
18. Gilman S, Low P, Quinn N, et al. Consensus statement on the diagnosis of multiple system atrophy. *Clin Auton Res* 1998;8:359-62.
19. Hughes AJ, Daniel SE, Kilford L, Lees AJ. Accuracy of clinical diagnosis of idiopathic Parkinson's disease: a clinico-pathological study of 100 cases. *J Neurol Neurosurg Psychiatry* 1992;55:181-4.
20. Rudd JH, Myers KS, Bansilal S, et al. Atherosclerosis inflammation imaging with 18F-FDG PET: carotid, iliac, and femoral uptake reproducibility, quantification methods, and recommendations. *J Nucl Med* 2008;49:871-8.
21. Tawakol A, Migrino RQ, Hoffmann U, et al. Noninvasive in vivo measurement of vascular inflammation with F-18 fluorodeoxyglucose positron emission tomography. *J Nucl Cardiol* 2005;12:294-301.
22. Valette H, Bottlaender M, Dollé F, et al. Imaging central nicotinic acetylcholine receptors in baboons with [<sup>18</sup>F]fluoro-A-85380. *J Nucl Med* 1999;40:1374-80.
23. Langer HF, Haubner R, Pichler BJ, Gawaz M. Radionuclide imaging. A molecular key to the atherosclerotic plaque. *J Am Coll Cardiol* 2008;52:1-12.
24. Cooke JP, Bitterman H. Nicotine and angiogenesis: a new paradigm for tobacco-related diseases. *Ann Med* 2004;36:33-40.
25. Cooke JP. Angiogenesis and the role of the endothelial nicotinic acetylcholine receptor. *Life Sci* 2007;80:2347-51.
26. Kawashima K, Yoshikawa K, Fujii YX, Moriaki Y, Misawa H. Expression and function of genes encoding cholinergic components in murine immune cells. *Life Sci* 2007;80:2314-9.
27. Gotti C, Clementi F. Neuronal nicotinic receptors: from structure to pathology. *Prog Neurobiol* 2004;74:363-96.
28. Macklin KD, Maus AD, Pereira EF, Albuquerque EX, Conti-Fine BM. Human vascular endothelial cells express functional nicotinic acetylcholine receptors. *J Pharmacol Exp Ther* 1998;287:435-9.
29. Heesch C, Weis M, Aicher A, Dimmeler S, Cooke JP. A novel angiogenic pathway mediated by non-neuronal nicotinic acetylcholine receptors. *J Clin Invest* 2002;110:527-36.
30. Moccia F, Frost C, Berra-Romani R, Tanzi F, Adams DJ. Expression and function of neuronal nicotinic ACh receptors in rat microvascular endothelial cells. *Am J Physiol Heart Circ Physiol* 2004;286:H486-91.
31. Wessler I, Kirkpatrick CJ, Racké K. The cholinergic 'pitfall': acetylcholine, a universal cell molecule in biological systems, including humans. *Clin Exp Pharmacol Physiol* 1999;26:198-205.
32. Cucina A, Sapienza P, Borrelli V, et al. Nicotine reorganizes cytoskeleton of vascular endothelial cell through platelet-derived growth factor BB. *J Surg Res* 2000;92:233-8.
33. Kiuchi K, Matsuoka M, Wu JC, et al. Mecamylamine suppresses Basal and nicotine-stimulated choroidal neovascularization. *Invest Ophthalmol Vis Sci* 2008;49:1705-11.
34. Li XW, Wang H. Non-neuronal nicotinic alpha 7 receptor, a new endothelial target for revascularization. *Life Sci* 2006;78:1863-70.
35. Kendziorra K, Wolf H, Meyer PM, et al. Decreased cerebral alpha4beta2\* nicotinic acetylcholine receptor availability in patients with mild cognitive impairment and Alzheimer's disease assessed with positron emission tomography. *Eur J Nucl Med Mol Imaging* 2011;38:515-25.
36. Altman R, Rutledge JC. The vascular contribution to Alzheimer's disease. *Clin Sci (Lond)* 2010;119:407-21.
37. Benamer HT, Grosset DG. Vascular parkinsonism: a clinical review. *Eur Neurol* 2009;61:11-5.
38. Kalra S, Grosset DG, Benamer HT. Differentiating vascular parkinsonism from idiopathic Parkinson's disease: a systematic review. *Mov Disord* 2010;25:149-56.

---

**Key Words:** arteries ■ multiple system atrophy ■ nicotinic acetylcholine receptors ■ Parkinson's disease ■ positron emission tomography.